

Water Stress Estimation from NDVI-Ts Plot and the Wet Environment Evapotranspiration

Daniela Girolimetto*, Virginia Venturini

Centre for Water and Environmental Studies, Universidad Nacional del Litoral,
Santa Fe, Argentina

Email: *dgirolimetto@fich.unl.edu.ar, vventurini@fich.unl.edu.ar

Received August 28, 2013; revised September 27, 2013; accepted October 8, 2013

Copyright © 2013 Daniela Girolimetto, Virginia Venturini. This is an open access article distributed under the Creative Commons Attribution License, which permits unrestricted use, distribution, and reproduction in any medium, provided the original work is properly cited.

ABSTRACT

In this work we present a new simple index to estimate water stress (WS) for different types of surfaces, from remotely sensed data. We derive a WS index, named WSI_{E_w} , modifying the Water Deficit Index (WDI) proposed by Moran *et al.* by using the wet environment evapotranspiration (E_w) instead of the potential evapotranspiration (E_{pot}) concept. Jiang and Islam model was used to simulate actual evapotranspiration (ET) and Priestley and Taylor equation to estimate E_w . The WSI_{E_w} results were compared to ground observations of ET, precipitation (PP), soil temperature (T_{soil}) and soil moisture (SM) in the Southern Great Plains-EEUU. Preliminary results suggest the method is sensitive to the water status of different surfaces. However, the WSI_{E_w} would range from 0 to 0.7, having a value of 0.4 for a dry surface with 5% of SM. The methodology is operationally simple and easy to implement since it requires only information from remote sensors.

Keywords: Water Stress; Water Status; Evapotranspiration; Remote Sensing

1. Introduction

The future of food depends largely on the water availability and strategic planning of the water resources. Therefore, to aid farmers to optimize the water uses is critical to maximize food production for the World. Nowadays vegetation WS indexes are extensively used in assisting farmer to maximize the crop yield when optimizing the irrigation system [1]. The need to monitor large areas motivated the development of WS indexes based on remotely sensed data. Indeed, the advent of the thermal infrared sensors allowed surface temperature (T_s) to be monitored and related to vegetation water deficits [2-5]. The correlation between surface temperature and water stress is based on the assumption that as a crop transpires, the leaves cool the air below them and the air temperature (T_a) drops [6]. Examples of successful water stress indexes are the Critical Temperature Variability (CTV) [5,7], the Crop Water Stress Index (CWSI) [3] and the Water Deficit Index (WDI) [8], among others.

Moran *et al.* [8] provided the theoretical derivation of the WDI based on the relative evaporation, defined as the ratio between actual evapotranspiration (ET) and poten-

tial evapotranspiration (E_{pot}). One of the main assumptions of the WDI is that soil and vegetation exchange energy and they cannot be analyzed separately [8]. This concept is particularly interesting for remote sensing applications where mix pixels, *i.e.* soil + vegetation, provide a single signal in every electromagnetic wavelength. The calculation is based on the vegetation index (VI) and T_s space, introduced by Price [9]. The most common VI used is the Normalized Difference Vegetation Index (NDVI) [10-12]. The IV- T_s space has also been used to estimate ET [13-15].

In this work we propose a new form of the WDI based on Jiang and Islam [16], and Priestley and Taylor [17] methods. The theoretical background provided by Moran *et al.* [8] is consistent to Jiang and Islam [16] methodology to estimate ET, therefore they are linkable in a single index called WSI_{E_w} .

2. Methodology

The background methodologies are the WDI published by Moran *et al.* [8] and Jiang and Islam [16] method. In this session both methods are briefly presented before we present the rationale behind the new index.

*Corresponding author.

2.1. The WDI Index

Moran *et al.* [8] discussed the validity of the CWSI theory for partially vegetated areas. The derivation of their new index is based on the interpretation of the trapezoidal shaped IV- (T_s-T_a) plot, where T_a is the air temperature.

Figure 1 exemplifies the borders of the trapezoid. The segment 1 - 3 represents the cold edge, with well watered conditions and vegetation cover ranging from bare soil to fully vegetated areas (NDVI ranging from 0 - 1). The segment 2 - 4, the warm edge, represents dry surfaces with vegetation varying from bare soil to full canopies. The segment 1 - 2 represents fully vegetated areas. Point 1 corresponds to well watered vegetation. Point 2 characterizes dry vegetation. The segment 3 - 4 represents bare soil [18]. Given the value of T_s-T_a at any point in the trapezoid (*i.e.* point B in **Figure 1**), the evaporation can be obtained by from the distances AB and BC.

The WDI considers two important assumptions associated to the relationship between IV and the difference T_s-T_a . First, the authors assume that the difference T_s-T_a is linearly related to percentage of vegetated area and the canopy and soil temperatures. Another important statement made by the authors is that given a certain net energy (R_n), the temperature of the foliage and soil are linearly related to the transpiration and evaporation respectively. Therefore, the variations in T_s-T_a would be associated to ET. Thus, for a partially vegetated area,

$$WDI = 1 - (ET/E_{pot}) \tag{1}$$

where (ET/E_{pot}) is the relative evaporation. E_{pot} is associated to a surface with unlimited water supply. The authors computed it with Penman-Monteith's equation [19] assuming the vegetation resistance (r_{cp}) closes to zero, without being canceled out.

Moran *et al.* [8] asserted that the VI has to be sensitive to the canopy variations and insensitive to spectral changes in soil background. Hence, the soil-adjusted vegetation index (SAVI) was the selected VI, and the linear

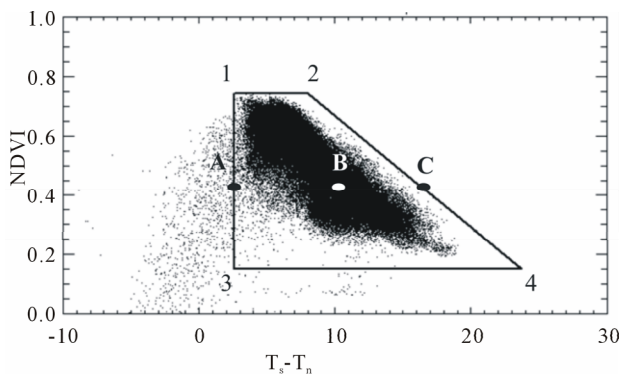


Figure 1. Trapezoidal diagram NDVI- (T_s-T_a) for date 04/05/2011.

edges of the SAVI- T_s space were adjusted to determine ET/E_{pot} . Details of the WDI are provided in Moran *et al.* [8].

2.2. Jiang and Islam Method

The Jiang-Islam's interpretation of the NDVI- T_s relationship provides the basis to estimate ET by modifying Priestley and Taylor's equation [17]. Jiang and Islam introduced a coefficient to account for unsaturated areas, which replaced the original Priestley and Taylor's coefficient (α). The resulting modified equation is,

$$ET_{J-I} = \phi \left[\frac{\Delta}{\Delta + \gamma} \right] (R_n - G) \tag{2}$$

where ϕ is Jiang-Islam's parameter, Δ is the slope of the saturation vapor pressure curve, γ is the psychrometric constant, R_n is the net radiation at the surface level = and G is soil heat flux.

The parameter ϕ varies from zero, for a dry bare soil surface, to α for a saturated or well vegetated surface, *i.e.* it becomes equal to Priestley and Taylor's equation. This parameter ϕ is calculated by a simple two-step linear interpolation between the sides of the NDVI- T_s triangle, as shown in **Figure 2**.

Jiang and Islam interpreted the upper edge, with high temperatures and low values of ϕ as the minimum value of ET for each class of NDVI, while the cold edge, associated with low T_s and maximum values of ϕ , represents maximum ET rate. Therefore, the value of ϕ vary within the limits of the triangle. Thus, NDVI- T_s plot is applied to derive ϕ by using the normalized temperature,

$$\phi_i = \alpha \frac{T_{max} - T_i}{T_{max} - T_{min}} \tag{3}$$

where T_{max} and T_{min} are the maximum and minimum T_s for a given vegetation class and T_i is the radiometric temperature for a given pixel.

In practice, the value of T_{max} is the temperature obtained extrapolating the upper edge to intersect the T_s

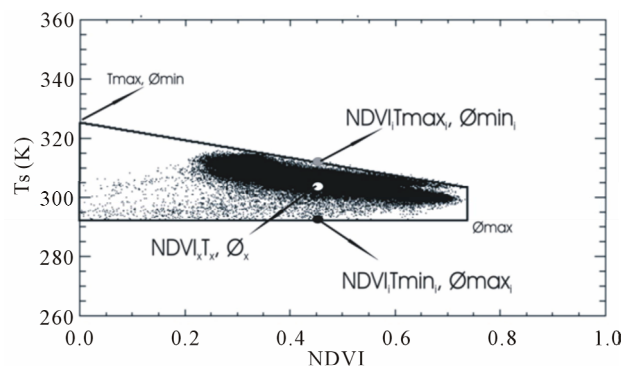


Figure 2. NDVI- T_s triangle space with upper and lower bonds and Jiang-Islam's parameters for date 04/05/2011.

axis (**Figure 2**) for a NDVI = 0, while T_{\min} is obtained as the average T_s of those pixels identified as water, *i.e.* with NDVI < 0. A full description of ϕ calculation can be found in Jiang and Islam [16].

2.3. The New Water Status Index (WSIE_w)

Moran *et al.* [8] related the WS with ET/E_{pot} (see Equation (1)), where E_{pot} was defined from the Penman-Monteith's equation [19] suggesting that the R_n , T_a , vapor pressure deficit (VPD) and the soil moisture (SM) are the main controlling factors for the stomata opening [2,4,8]. One of the main assumption of this model is that r_{cp} tends to zero. This E_{pot} definition is closer to a wet environment evapotranspiration (E_w) concept than to a truly potential concept, where the energy is maximum, the surrounding air is dry while the surface is saturated [20]. Hence, for a given atmospheric condition and unlimited water supply, the soil+ plant complex will evapotranspire at its maximum rate according to the available energy. In this case, the maximum rate of ET is given by E_w [17,21-23].

The vegetation stress is mainly caused by deficit of moisture at the root zone. In the absence of watering, the moisture content in the root zone will be reduced as a result of crop intake. In turn, water stress causes the closure of the stoma of the plants and hence a reduction in the transpiration rate. Then, the ratio ET/E_w is a good indicator of evapotranspiration deficit [24]. Thus, E_w can replace the E_{pot} in Equation (1), and the WDI (see Equation (1)) can be written as,

$$\text{WDI} = 1 - \frac{ET}{E_w} \quad (4)$$

In this new form of WDI, ET can be replaced by the Equation (2) [16] and E_w by the Priestley-Taylor equation. The new index, WSI_{E_w} in terms of the parameters ϕ and α is:

$$WSI_{E_w} = 1 - \frac{\phi}{\alpha} \quad (5)$$

replacing ϕ by equation 3, the WSI_{E_w} becomes,

$$WSI_{E_w} = 1 - \frac{T_{\max} - T_i}{T_{\max} - T_{\min}} = \frac{T_i - T_{\min}}{T_{\max} - T_{\min}} \quad (6)$$

where T_i is the radiometric temperature for a given pixel and T_{\max} and T_{\min} are the Jiang and Islam's parameters.

Operational robust methods could be achieved with purely remotely sensed data, as we propose here. In this case, T_a and the VPD are not explicitly required to compute the new index. The WSI_{E_w} does not require the understanding of the crop type biophysical functions under specific climates. The WSI_{E_w} could be calculated from data recorded from current satellite missions, such as NOAA series, EOS-Terra and EOS-Aqua. In this work

we applied to WSI_{E_w} to the Southern Great Plains (SPG), using MODIS images and comparing the results with observations.

3. Study Area and Data

3.1. Study Area

The SGP region of US is a flat terrain, heterogeneous land cover with seasonal variation in temperature and humidity. It extends over the State of Oklahoma and southern part of Kansas, running from longitude 95.5°W to 99.5°W and from latitude 34.5°N to 38.5°N.

This region has relatively extensive and well distributed coverage of ground stations, maintained by the Atmospheric Radiation Measurement (ARM) program. The stations are widely distributed over the whole domain (**Figure 3**). E8 and E22 are located in a grazed rangeland region, E4 in an ungrazed rangeland area, E13 is positioned in a region with pasture and wheat, E7, E9, E15, E20 and E27 are located in pastures. E18 and E19 are in ungrazed pasture area, E12 is located in a native prairie, E10 is in alfalfa, E16 is in wheat region and E2 is in grass region.

3.2. Data and Images

The Energy Balance Bowen Ratio (EBBR) system compute 30-min estimates of the sensible and latent heat vertical fluxes at the local scale. Flux estimates are calculated from observations of net radiation, soil surface heat flux, and the vertical gradients of temperature and relative humidity. The instruments and measurement applications are well established and have been used for validation purposes in many studies [22,23,25,26]. Further information about the ARM EBBR data and methodology is available at <http://www.arm.gov>.

MODIS is one of the instruments on board EOS-Terra and EOS-Aqua satellites <http://modis.gsfc.nasa.gov/> [27,28].

Daytime MODIS-Aqua images for nine days in years 2009, 2010 and 2011 in spring and summer with at least 82% of the study area free of clouds were selected. **Table 1** summarizes the image information including date, day of the year, satellite overpass time and image quality. The product MYD02 and MYD11 were used in this work. MYD02 provides corrected radiance, reflectance and geolocations for 36 bands and MYD11 provides T_s images on a daily base [23,29,30].

4. Results

4.1. Preprocessing

The MODIS images were georeferenced from the Latitude and Longitude associate to each pixel. The study area was pulled out of each image and geographically projected in a grid of 445 columns by 445 rows, with

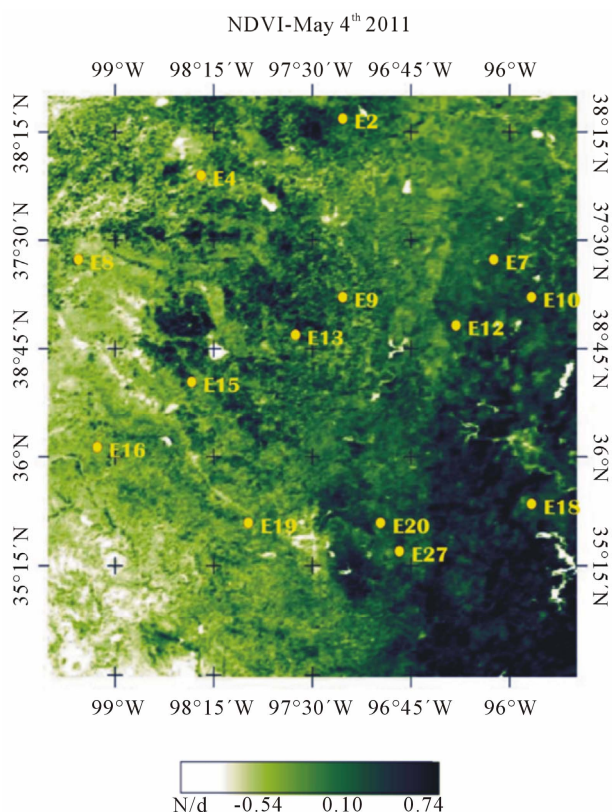


Figure 3. Southern Great Plains and ground station locations.

Table 1. Date day of the year overpass time and image quality of the nine study days.

Date	Day of the year (DOY)	Overpass time (UTC)	Image quality (% clouds)
April 6th 2011	96	19:30	15
May 4th 2011	124	19:55	1
May 26th 2011	146	19:20	2
May 29th 2011	149	19:50	1
June 5th 2011	156	19:55	14
April 10th 2010	100	19:40	5
June 4th 2010	155	19:45	18
June 5th 2009	156	19:25	14
August 22nd 2009	234	19:35	11

pixels of approximately 1 km resolution. The reflectance of the red band (R) and near-infrared band (NIR) were obtained at the top of the atmosphere. The R and NIR images were used to obtain the NDVI,

$$\text{NDVI} = \frac{\text{NIR} - \text{R}}{\text{R} + \text{NIR}} \quad (7)$$

The NDVI- T_s spaces were plotted to obtain Jiang-Islam's parameters (T_{\max} and T_{\min}) and then obtain the WSI_{Ew} by Equation (6). Then, the WSI_{Ew} was validated with field data and contrasted with variables that

are commonly associated to water stress.

Given that the WS is not directly measurable, we computed the WS with Equation (4) using ET ground observations (ET_{obs}) and Priestley and Taylor's equation as follows,

$$WS_{obs} = 1 - \frac{ET_{obs}}{\alpha \frac{\Delta}{\Delta + \gamma} (R_n^{Obs} - G^{Obs})} \quad (8)$$

where R_n^{Obs} is the net radiation observed at the Bowen ratio stations, G^{Obs} is the ground data of soil head flux, Δ and γ were computed from observed air temperature and atmospheric pressure.

WSI_{Ew} was compared with the WS_{obs} and WDI obtained from NDVI- $(T_s - T_a)$ space. Finally, in order to analyze the applicability of WSI_{Ew} we compared it with different variables associated to the stress.

4.2. WS Results

The regional statistic of WSI_{Ew} , *i.e.* maximum, mean and standard deviation, for each of the days are shown in **Table 2**.

The regional minimum is always equal to 0.0, since Jiang and Islam's method [16] requires free water pixels to estimate T_{\min} . The minimum temperature represents $ET = E_w$, *i.e.* no-stress condition; thus, no-stress pixels are always present in this methodology. The regional maximum ranges from 0.50 and 0.72. The mean values of WSI_{Ew} vary from 0.14 to 0.42. For all the study days, the standard deviation is lower than 0.12 suggesting little regional dispersion around the mean of WSI_{Ew} . Wang *et al.* [12] analyzed the phenological cycle of winter wheat under irrigation in the North China Plain. The authors associated CWSI values lower than 0.34 to no stress conditions. Kar and Kumar [31] analyzed the CWSI in peanut crops under irrigation. They found CWSI values between 0.61 and 0.63 just before the application of irrigation. Hence, the regional WSI_{Ew} obtained here are comparables with those published by other authors. How-ever further analysis is needed to characterize the

Table 2. regional statistics WSI_{Ew} (values maximum, average and standard deviation).

Dia	Average	Max	Standard Deviation
April 6th 2011	0.30	0.54	0.080
May 4th 2011	0.42	0.72	0.098
May 26th 2011	0.23	0.68	0.118
May 29th 2011	0.27	0.60	0.099
June 5th 2011	0.34	0.66	0.114
April 10th 2010	0.32	0.70	0.068
June 4th 2010	0.26	0.52	0.101
June 5th 2009	0.23	0.50	0.090
August 22nd 2009	0.14	0.51	0.067

WSI_{E_w} valid range.

Results of WSI_{E_w} and WS_{obs} were compared. The bias was obtained as $\sum(WS_{obs} - WSI_{E_w})/n$ and RMSE as $(\sum(WS_{obs} - WSI_{E_w})^2/n)^{0.5}$, where n is the number of observations. These statistics show bias of 0.05 and RMSE of 0.120, which represents approximately 24% of the mean WS (assuming a mean value of 0.5).

It is not evident how to validate the stress indexes from the literature revised here. For instance, Colaizzi *et al.* [32] compared the WDI and the soil water deficit index (SWDI). They found values of RMSE lower than 0,143 (29% of the mean) and bias lower than 0.112, consistent with the results presented here. In both cases, the RMSE are of the same order indicating that the method's errors are about 30% of the mean.

The comparison between WDI and WSI_{E_w} remarks the differences between both models, with a bias of 0.28 and RMSE of 0.27 (54%). These results could be due to the separation between the bulk of the pixels and the dry border in the trapezoid (see **Figure 1**). These differences would be related to the differences in the E_w and E_{pot} concepts already explained in Section 2.3.

The WSI_{E_w} results were also compared with records of different variables that index water stress. **Figure 4** presents the WSI_{E_w} versus observed SM (at 5 cm below the surface).

There is a well defined inverse relationship between the SM and the WSI_{E_w} (**Figure 4**) with a coefficient of determination (R^2) equal to 0.52. The dissimilar spatial resolution of both data sets may be the cause of the dispersion observed in **Figure 4**. Certainly the WSI_{E_w} is calculated as a result of the signal from $1 \text{ km} \times 1 \text{ km}$ pixel while the ancillary data are representative of few meters around the point station [30]. Nevertheless, values of SM of 5%, characteristic of low moisture in most soils, correspond to WSI_{E_w} of about 0.45 while a SM of 30%, *i.e.* a well watered surface, could be associated to a WSI_{E_w} of 0.2.

Figure 5 displays WSI_{E_w} versus T_{soil} (at 5 cm below the surface). These relationship showed a $R^2 = 0.72$. It should be noted that ϕ is a dimensionless temperature, what may explain the relationship with the soil temperature presented in **Figure 5**. Patel *et al.* [33] examined the potential of using canopy-air temperature difference ($T_c - T_a$) for assessing the crop water status. The authors correlated $T_c - T_a$ with SM (at 15 cm) with a $R^2 = 0.59$. Fensholt and Sandholt [34] found a $R^2 = 0.48$ when comparing the Shortwave Infrared Water Stress Index (SIWSI) with soil moisture observed *in situ*.

The inverse relationship between observed ET_{obs} and calculated WSI_{E_w} presented in **Figure 6** is noteworthy, given that the ET records are independent to ET_{j-1}/E_w . In general, the WSI_{E_w} seems to capture the surface water stress condition well.

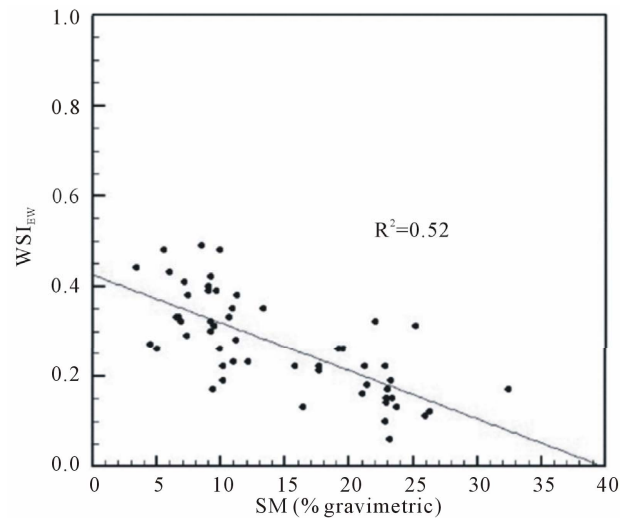


Figure 4. WSI_{E_w} vs observed SM (at 5 cm).

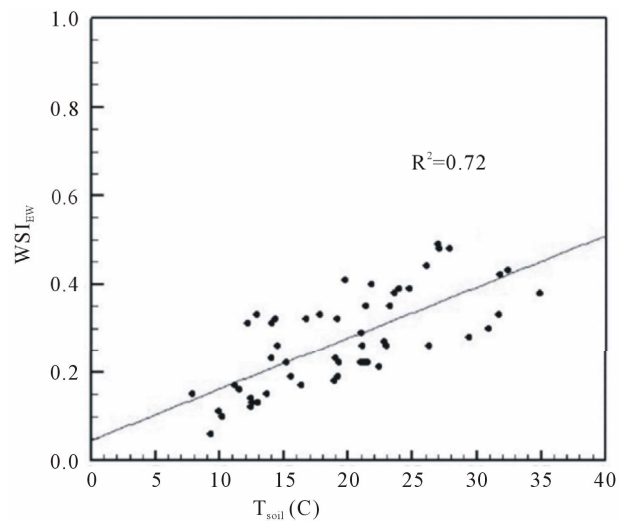


Figure 5. WSI_{E_w} vs observed Tsoil (at 5 cm).

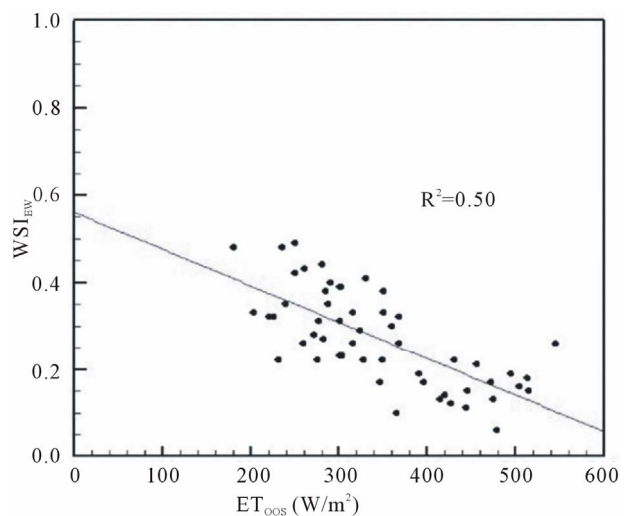


Figure 6. WSI_{E_w} vs observed ET.

The WSI_{Ew} was compared with the rainfall accumulated five days prior to the analyzed dates (PP). The comparison is shown in **Figure 7** where the decrease of WS when rainfall increases is observed ($R^2 = 0.62$). As the surface gets humid more water is available for ET and the ratio ET/E_{pot} tends to one. Thus, the stress decreases with the precipitation increase.

Wang *et al.* [12] studied the wheat in the plain of China. They associated the wheat low stress to high rainfall events. The authors concluded that a good wheat harvest was obtained for CWSI lower than 0.34, representing a not-stress condition.

Figure 8 shows the comparison of WSI_{Ew} with soil moisture and PP for station E12. The SM observed at 5 cm is supplied by PP and represent the roots water availability [34], thus any reduction of PP, causes a decrease in the SM and it is expected to cause an increase of the WSI_{Ew} .

Finally, **Figure 9** shows the WSI_{Ew} map for the SGP for the May 4th 2011, where we observed the stress would decrease from West to East. In general, the mountain areas present WSI_{Ew} of 0.7 and the prairies at the East show values of WSI_{Ew} about 0.3. The black areas are cloudy masked pixel [16,30].

4.3. Sensitivity Analysis

T_{max} is the main parameter of the index presented in this paper, thus the sensitivity of the WSI_{Ew} to variation of T_{max} is analyzed here.

Different methods to draw the warm and cold edge of the triangle [10,11] would render different values of T_{max} in Jiang-Islam method. Thus, we apply the First Order Analysis to estimate the effect of T_{max} on WSI_{Ew} variance.

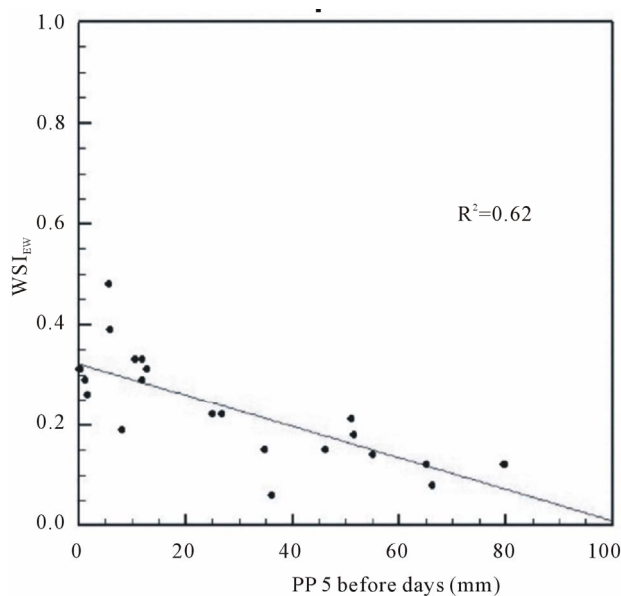


Figure 7. WSI_{Ew} vs PP (mm).

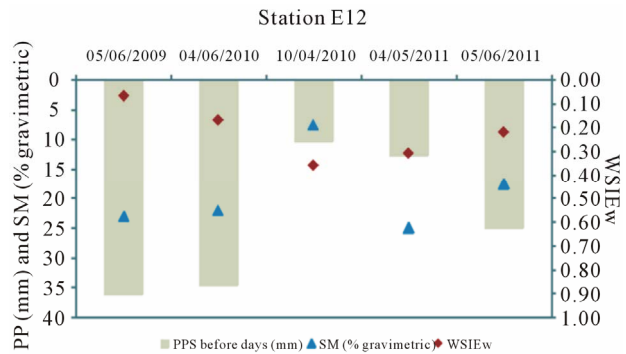


Figure 8. WSI_{Ew} vs SM and PP for station E12.

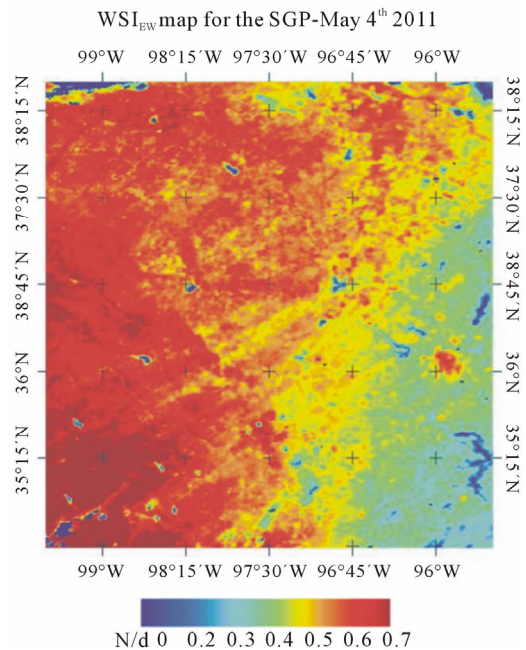


Figure 9. WSI_{Ew} map for the SGP for the May 4th 2011.

$$S^2_{WSI_{Ew}} = \left(\frac{T_{min} - T_i}{(T_{max} - T_{min})} \right)^2 S^2_{T_{max}} \tag{9}$$

The results of applying Equation (9) with different T_{min} , T_{max} , T_i statistic and assuming that $S^2_{T_{max}}$ varies from 1% to 15%, suggested that $S^2_{WSI_{Ew}}$ varies from 2.5% to 30% approximately. These results indicate that variations up 10% of T_{max} would cause errors of about 15% in WSI_{Ew} .

5. Discussion

Several methods have been developed to determine the WS from observations of the T_s [2-5]. The index proposed by Moran *et al.* [8], based on the relative evaporation concept, is widely applied all over the world [18,32, 35]. In this work we presented a modification of WDI proposed by Moran *et al.* [8]. The new index replaces the

E_{pot} used in the original formulation for the E_w concept. Given that $E_w \leq E_{\text{pot}}$ [20], the ratio ET/E_{pot} is smaller than ET/E_w , yielding two WS indexes that point out different causes of vegetation stress. The WSI_{E_w} would only consider the stress due to water shortness in the root zone while the WDI would also reflect the stoma closure cause by the atmospheric and radiation effects.

The WDI required field information (observations of R_n , G , wind speed, T_a) to establish the end-points that define the trapezoid (**Figure 1(a)**). If such information was not available, it would be necessary to guess them from each analyzed image; *i.e.* indentifying groups of pixels that represent the natural conditions of the end-points. Guessing the extreme points creates uncertainty in the interpretations of the diagrams [35]. The WSI_{E_w} also requires determination of the triangle borders, however in this case, the source of error would be mainly associated with definition of T_{max} .

The WSI_{E_w} is another “thermal index” with the form of a normalized temperature, *i.e.*

$$WSI_{E_w} = (T_i - T_{\text{min}}) / (T_{\text{max}} - T_{\text{min}})$$

[30]. T_{max} is the temperature for a hypothetical dry bare soil pixel and T_{min} is the temperature for a saturated pixel. It must be noted that the T_{max} is not the maximum thermal infrared of the image or maximum canopy temperature; on contrast, it is a “hypothetical” maximum temperature. It is usually found in the literature thermal stress indices calculated as a normalized T_s , the difference between the methods is given the extreme temperatures estimation. For instance, Galleguillos *et al.* [18] used the WDI to derive the daily ET. The authors assumed that T_a is constant in the study area and they estimated the maximum and minimum T_s from the energy balance. Wang *et al.* [35] made use of the WDI to estimate soil moisture. These authors explored the T_s -EVI (Enhanced Vegetation Index) space to determine the minimum and maximum values of T_s .

The relationship between the WSI_{E_w} and SM ($R^2 = 0.52$) provided interesting information. In **Figure 3(a)** we observe that a soil with 5% of moisture matches a WSI_{E_w} of about 0.45. On the other extreme, a SM of 30% agrees with a WSI_{E_w} of 0.1. In other words, the WSI_{E_w} would not get close to 1 although the SM indicates a dry surface.

We compare the WSI_{E_w} with the rainfall accumulated five days prior to the analyzed dates, observing that the WS decreases as precipitation increases, however there is no sufficient analysis about irrigation fields and precipitation spatial distribution in this work to deepen the conclusions about the WSI_{E_w} range of variation.

The advantage of this new formulation is that there is no need of crop-field observations, yet overestimated T_{max} values might yield an underestimated water stress condition. Thus, a T_{max} significantly larger than the actual

dry soil temperature, would not index the stress with a WSI_{E_w} value close to 1, as it would be expected by the end-users. In general, the WSI_{E_w} shows significant correlations with water stress indicators.

The WSI_{E_w} is applicable to different satellite missions and requires minor image processing. The new index can be very useful for end users who require quick and easy methods of application.

REFERENCES

- [1] R. López-López, R. Arteaga-Ramírez, M. A. Vázquez-Peña, I. López-Cruz and I. Sánchez-Cohen, “Índice de Estrés Hídrico Como un Indicador del Momento de Riego en Cultivos Agrícolas,” *Agricultura Técnica en México*, Vol. 35, No. 1, 2009, pp. 92-106.
- [2] R. D. Jackson, S. B. Idso, R. J. Reginato and W. L. Ehler, “Crop Temperature Reveals Stress,” *Crop Soils*, Vol. 29, No. 8, 1977, pp. 10-13.
- [3] R. D. Jackson, “Canopy Temperature and Crop Water Stress,” In D. Hillel, Eds., *Advances in Irrigation*, Academic Press, New York, 1982, pp. 43-85.
- [4] S. B. Idso, “Non-Water-Stressed Baselines: A Key to Measuring and Interpreting Plant Water Stress,” *Agricultural Meteorology*, Vol. 27, No. 1-2, 1982, pp. 59-70. [http://dx.doi.org/10.1016/0002-1571\(82\)90020-6](http://dx.doi.org/10.1016/0002-1571(82)90020-6)
- [5] K. L. Clawson and B. L. Blad, “Infrared Thermometry for Scheduling Irrigation of Corn,” *Agronomy Journal*, Vol. 74, No. 3, 1982, pp. 311-316.
- [6] M. Usman, A. Ahmad, S. Ahmad, M. Arshad, T. Khaliq, A. Wajid, K. Hussain, W. Nasim, T. Mehmood Chattha, R. Trethowan and G. Hoogenboom, “Development and Application of Crop Water Stress Index for Scheduling Irrigation in Cotton (*Gossypium hirsutum* L.) under Semi-arid Environment,” *Journal of Food Agriculture and Environment*, Vol. 7, No. 3-4, 2009, pp. 386-391.
- [7] B. L. Blad, D. G. Gardner, N. J. Watts and N. J. Rosenberg, “Remote Sensing of Crop Moisture Status,” *Remote Sensing*, Quart. 3, 1981, pp. 4-20.
- [8] M. S. Moran, T. R. Clarke, Y. Inoue and A. Vidal, “Estimating Crop Water Deficit Using the Relation between Surface-Air Temperature and Spectral Vegetation Index,” *Remote Sensing Environment*, Vol. 49, No. 3, 1994, pp. 246-263. [http://dx.doi.org/10.1016/0034-4257\(94\)90020-5](http://dx.doi.org/10.1016/0034-4257(94)90020-5)
- [9] J. C. Price, “Using Spatial Context in Satellite Data to Infer Regional Scale Evapotranspiration,” *IEEE Transactions on Geoscience and Remote Sensing*, Vol. 28, No. 5, 1990, pp. 940-948. <http://dx.doi.org/10.1109/36.58983>
- [10] T. N. Carlson, R. R. Gillies and T. J. Schmugge, “An Interpretation of Methodologies for Indirect Measurement of Soil Water Content,” *Agricultural and Forest Meteorology*, Vol. 77, No. 3-4, 1995, pp. 191-205. [http://dx.doi.org/10.1016/0168-1923\(95\)02261-U](http://dx.doi.org/10.1016/0168-1923(95)02261-U)
- [11] I. Sandholt, K. Rasmussen and J. Andersen, “A Simple Interpretation of the Surface Temperature/Vegetation Index Space for Assessment of Surface Moisture Status,”

- Remote Sensing Environment*, Vol. 49, No. 3, 2002, pp. 246-263.
- [12] L. Wang, G. Y. Qiu, X. Zhang and S. Chen, "Application of a New Method to Evaluate Crop Water Stress Index," *Irrigation Science*, Vol. 24, No. 1, 2005, pp. 49-54. <http://dx.doi.org/10.1007/s00271-005-0007-7>
- [13] R. R. Gillies, T. N. Carlson, J. Cui, W. P. Kustas and K. S. Humes, "A Verification of the 'Triangle' Method for Obtaining Surface Fluxes from Remote Measurements of the Normalized Difference Vegetation Index (NDVI) and Surface Radiant Temperature," *International Journal of Remote Sensing*, Vol. 18, No. 15, 1997, pp. 3145-3166. <http://dx.doi.org/10.1080/014311697217026>
- [14] L. Jiang and S. Islam, "A Methodology for Estimation of Surface Evapotranspiration over Large Areas Using Remote Sensing Observations," *Geophysical Research Letters*, Vol. 26, No. 17, 1999, pp. 2773-2776. <http://dx.doi.org/10.1029/1999GL006049>
- [15] S. Stisen, I. Sandholt, A. Norgaard, R. Fensholt and K. H. Jensen, "Combining the Triangle Method with Thermal Inertia to Estimate Regional Evapotranspiration—Applied to MSG-SEVIRI Data in the Senegal River Basin," *Remote Sensing Environment*, Vol. 112, No. 3, 2008, pp. 1242-1255. <http://dx.doi.org/10.1016/j.rse.2007.08.013>
- [16] L. Jiang and S. Islam, "Estimation of Surface Evaporation Map over Southern Great Plains Using Remote Sensing Data," *Water Resources Research*, Vol. 37, No. 2, 2001, pp. 329-340. <http://dx.doi.org/10.1029/2000WR900255>
- [17] C. H. B. Priestley and R. J. Taylor, "On the Assessment of Surface Heat Flux and Evaporation Using Large-Scale Parameters," *Monthly Weather Review*, Vol. 100, No. 2, 1972, pp. 81-92. [http://dx.doi.org/10.1175/1520-0493\(1972\)100<0081:OTAOSH>2.3.CO;2](http://dx.doi.org/10.1175/1520-0493(1972)100<0081:OTAOSH>2.3.CO;2)
- [18] M. Galleguillos, F. Jacob, L. Prévot, A. French and P. Lagacherie, "Comparison of Two Temperature Differencing Methods to Estimate Daily Evapotranspiration over a Mediterranean Vineyard Watershed from ASTER Data," *Remote Sensing Environment*, Vol. 115, No. 6, 2011, pp. 1326-1340. <http://dx.doi.org/10.1016/j.rse.2011.01.013>
- [19] J. L. Monteith and M. Unsworth, "Principles of Environmental Physics," 2nd Edition, Butterworth-Heinemann, Burlington, 1990, 304p.
- [20] R. J. Granger, "An Examination of the Concept of Potential Evaporation," *Journal of Hydrology*, Vol. 111, No. 1-4, 1989, pp. 9-19. [http://dx.doi.org/10.1016/0022-1694\(89\)90248-5](http://dx.doi.org/10.1016/0022-1694(89)90248-5)
- [21] W. Brutsaert and H. Stricker, "An Advection-Aridity Approach to Estimate Actual Regional Evapotranspiration," *Water Resources Research*, Vol. 15, No. 2, 1979, pp. 443-450. <http://dx.doi.org/10.1029/WR015i002p00443>
- [22] V. Venturini, S. Islam and L. Rodríguez, "Estimation of Evaporative Fraction and Evapotranspiration from MODIS Products Using a Complementary Based Model," *Remote Sensing Environment*, Vol. 112, No. 1, 2008, pp. 132-141. <http://dx.doi.org/10.1016/j.rse.2007.04.014>
- [23] V. Venturini, L. Rodríguez and G. Bisht, "A Comparison among Different Modified Priestley and Taylor's Equations to Calculate Actual Evapotranspiration with MODIS Data," *International Journal of Remote Sensing*, Vol. 32, No. 5, 2010, pp. 1319-1338. <http://dx.doi.org/10.1080/01431160903547965>
- [24] J. V. Straschnoy, C. M. Di Bella, F. R. Jaimes, P. A. Oricchio and C. M. Rebella, "Caracterización Espacial del Estrés Hídrico y de las Heladas en la Región Pampeana a Partir de Información Satelital y Complementaria," *Revista de Investigaciones Agropecuarias*, Vol. 35, No. 2, 2006, pp. 117-141.
- [25] W. J. Shuttleworth, "Insight from Large-Scale Observational Studies of Land/Atmosphere Interactions," *Surveys in Geophysics*, Vol. 12, No. 1-3, 1991, pp. 3-30. <http://dx.doi.org/10.1007/BF01903410>
- [26] J. M. Lewis, "The Story behind the Bowen Ratio," *Bulletin of the American Meteorological Society*, Vol. 76, No. 12, 1995, pp. 2433-2443. [http://dx.doi.org/10.1175/1520-0477\(1995\)076<2433:TSBTBR>2.0.CO;2](http://dx.doi.org/10.1175/1520-0477(1995)076<2433:TSBTBR>2.0.CO;2)
- [27] C. O. Justice, J. R. G. Townshend, E. F. Vermote, E. Masuoka, R. E. Wolfe, N. Saleous, D. P. Roy and J. T. Morisette, "An Overview of MODIS Land Data Processing and Product Status," *Remote Sensing Environment*, Vol. 83, No. 2, 2002, pp. 3-15.
- [28] E. F. Vermote, N. Z. Saleous and C. O. Justice, "Atmospheric Correction of MODIS Data in the Visible to Middle Infrared: First Results," *Remote Sensing Environment* Vol. 83, No. 2, 2002, pp. 97-111.
- [29] Z. Wan and J. A. Dozier, "A Generalized Split-Window Algorithm for Retrieving Land-Surface Temperature from Space," *IEEE Transactions on Geoscience and Remote Sensing*, Vol. 34, No. 4, 1996, pp. 892-905. <http://dx.doi.org/10.1109/36.508406>
- [30] V. Venturini, G. Bisht, S. Islam and L. Jiang, "Comparison of Evaporative Fractions Estimated from AVHRR and MODIS Sensors over South Florida," *Remote Sensing Environment*, Vol. 93, No. 1-2, 2004, pp. 77-86. <http://dx.doi.org/10.1016/j.rse.2004.06.020>
- [31] G. Kar and A. Kumar, "Surface Energy Fluxes and Crop Water Stress Index in Groundnut under Irrigated Ecosystem," *Agricultural and Forest Meteorology*, Vol. 146, No. 1-2, 2007, pp. 94-106. <http://dx.doi.org/10.1016/j.agrformet.2007.05.008>
- [32] P. D. Colaizzi, E. M. Barnes, T. R. Clarke, C. Y. Choi, M. Peter, P. M. Waller, J. Haberland and M. Kostrzewski, "Water Stress Detection Under High Frequency Sprinkler Irrigation with Water Deficit Index," *Journal of Irrigation and Drainage Engineering*, Vol. 129, No. 1, 2003, pp. 36-43.
- [33] N. R. Patel, A. N. Mehta and A. M. Shekh, "Canopy Temperature and Water Stress Quantification in Rainfed Pigeonpea (*Cajanus cajan* (L.) Millsp.)," *Agricultural and Forest Meteorology*, Vol. 109, No. 3, 2001, pp. 223-232. [http://dx.doi.org/10.1016/S0168-1923\(01\)00260-X](http://dx.doi.org/10.1016/S0168-1923(01)00260-X)
- [34] R. Fensholt and I. Sandholt, "Derivation of a Shortwave Infrared Water Stress Index from MODIS Near- and Shortwave Infrared Data in a Semiarid Environment,"

- Remote Sensing Environment*, Vol. 87, No. 1, 2003, pp. 111-121. <http://dx.doi.org/10.1016/j.rse.2003.07.002>
- [35] W. Wang, D. Huang, X. G. Wang, Y. R. Liu and F. Zhou, "Estimation of Soil Moisture Using Trapezoidal Relationship between Remotely Sensed Land Surface Temperature and Vegetation Index," *Hydrology and Earth System Sciences*, Vol. 15, No. 5, 2011, pp. 1699-1712. <http://dx.doi.org/10.5194/hess-15-1699-2011>